Published in final edited form as:

Inorg Chem. 2019 May 20; 58(10): 6790–6795. doi:10.1021/acs.inorgchem.9b00248.

Rattling Behavior in a Simple Perovskite $NaWO_3$

Yuya Ikeuchi[†], **Hiroshi Takatsu**[†], **Cédric Tassel**[†], **Craig M. Brown**[‡], **Taito Murakami**[†], **Yuki Matsumoto**[†], **Yoshihiko Okamoto**[§], **Hiroshi Kageyama**[*,†]

[†]Graduate School of Engineering, Kyoto University, Kyoto 615-8510, Japan

[‡]Center for Neutron Research National Institute of Standards and Technology Gaithersburg, Maryland 20899, United States

[§]Department of Applied Physics, Nagoya University, Nagoya 464-8603, Japan

Abstract

Rattling phenomena have been observed in materials characterized by a large cage structure but not in a simple ABO_3-type perovskite because the size mismatch, if it exists, can be relieved by octahedral rotations. Here, we demonstrate that a stoichiometric perovskite oxide $NaWO_3$, prepared under high pressure, exhibits anharmonic phonon modes associated with low-energy rattling vibrations, leading to suppressed thermal conductivity. The structural analysis and the comparison with the ideal perovskite KWO_3 without rattling behavior reveal that the presence of two crystallographic Na1 (2*a*) and Na2 (6*b*) sites in $NaWO_3$ (space group $Im\bar{3}$) accompanied by three in-phase WO_6 octahedral ($a^+a^+a^+$) rotations generates an open space $\Delta \sim 0.5$ Å for the latter site, which is comparable with those of well-known cage compounds of clathrates and filled skutterudites. The observed rattling in $NaWO_3$ is distinct from a quadruple perovskite $AA'_3B_4O_{12}$ (A, A′: transition metals) where the A (2*a*) site with lower multiplicity is the rattler. The present finding offers a general guide to induce rattling of atoms in pristine ABO_3 perovskites.

Graphical Abstract

[*]Corresponding Author kage@scl.kyoto-u.ac.jp.

The authors declare no competing financial interest.

ASSOCIATED CONTENT

Supporting Information

The Supporting Information is available free of charge on the ACSPublicationswebsite at DOI: 10.1021/acs.inorgchem.9b00248. Detailed information on sample preparation, measurements of physical properties (electrical resistivity, specific heat, and thermal conductivity), and analysis of specific heat (PDF)

Accession Codes

CCDC 1893481 contains the supplementary crystallographic data for this paper. These data can be obtained free of charge via www.ccdc.cam.ac.uk/data_request/cif, or by emailing data_request@ccdc.cam.ac.uk, or by contacting The Cambridge Crystallographic Data Centre, 12 Union Road, Cambridge CB2 1EZ, UK; fax: +44 1223 336033.

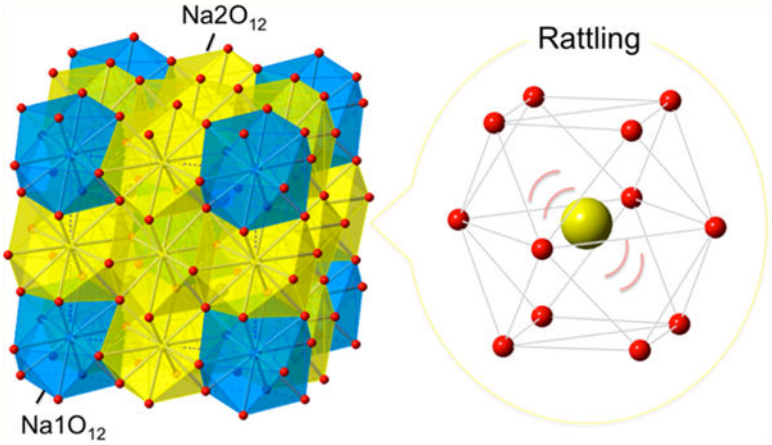

INTRODUCTION

Inorganic solids with a network of polyhedral cages that host guest cations show interesting properties associated with characteristic phonon modes.[1–4] When guest cations are smaller relative to the space inside the cage, a local and anharmonic vibration, or “rattling”, occurs, leading to strong scattering of long wavelength acoustic phonons in clathrates (e.g., $Sr_8Ga_{16}Ge_{30}$),[5,6] superconductivity with strong electron–phonon coupling in β-pyrochlore $IKOs_2O_6$,[7–9] and heavy Fermion states in filled skutterudites (e.g., $SmOs_4Sb_{12}$).[10–13] It has been widely believed that the rattling vibration suppresses the lattice thermal conductivity, κ_L, resulting in the enhancement of thermoelectric efficiency.[14–16] Quasi-harmonic interaction between the cage and guest cation is also proposed.[17] These features have stimulated numerous studies toward exotic physical properties coupled with rattling vibrational modes, such as high efficiency thermoelectric materials with low κ_L.

Perovskite ABO_3 is the most studied system in materials science because of the richness in chemical and physical properties including superconductivity,[18] colossal magneto-resistivity,[19] and ferroelectricity.[20] The diversity of properties arises from the ability of perovskite compounds to take various cations at the A and B sites,[21] along with the substitution of oxide site by other anions.[22] In addition, octahedral rotation of various patterns causes the deviation of ∠B–O–B angle from 180° in the ideal perovskite, which influences orbital overlap, superexchange interactions, and electron hopping between neighboring B sites. Here, the relief of size mismatch is the origin of octahedral rotations: when the Goldschmidt tolerance factor is smaller than 1, BO_6 octahedra rotate to satisfy the necessary the A site cation environment, leading to structural distortion from a cubic perovskite (space group: $Pm\bar{3}m$).[21] Octahedral rotations match almost any A site sizes, leading to dense structures and therefore leaving little “open space” for rattling to occur. Recently, Tanaka et al. reported several quadruple perovskite oxides, $ACu_3V_4O_{12}$ (A = Mn, Cu).[23,24] In general, the A′ ions in $AA'_3B_4O_{12}$ are Jahn–Teller active transition metals (e.g., Cu^{2+} and Mn^{3+}), and extensive BO_6 octahedral tilting permits square-planar $A'O_4$ coordination.[25] The resultant A site is 12-fold coordinated typically occupied by large alkaline earth metals (e.g., La), but when it is occupied by small transition metal ions, a rattling phenomenon emerges, as seen from a large atomic displacement parameter (ADP) and Einstein-like specific heat.[23,24]

In this paper, we report the high-pressure synthesis of a stoichiometric tungsten bronze Na_xWO_3 ($x = 1$). Na_xWO_3 has been extensively studied for decades, and a perovskite structure with $a^+a^+a^+$ octahedral rotation (space group: $Im\bar{3}$) is found in a high concentration regime ($x \geq 0.8$).[26–29] However, there remains an uncertainty about its Na composition, as will be shown later. The present study follows our recent work on K_xWO_3, where the high-pressure method expanded the x amount, forming a stoichiometric tetragonal phase $K_{0.6}WO_3$ and a cubic (perovskite) one KWO_3.[30] Quite unexpectedly, we observed rattling behavior in this *pristine* perovskite $NaWO_3$ but not in KWO_3. We discuss the origin of the rattling phenomenon in NWO_3 by considering crystal structures and physical properties, in comparison with the 1:3 ordered quadruple perovskite $AA'_3B_4O_{12}$. A general guideline to the rattling phenomenon in perovskite is presented.

EXPERIMENTAL PROCEDURE

Polycrystalline samples of Na_xWO_3 ($x = 0.5, 0.6, 0.75, 0.8, 1.0$) were prepared using a high-pressure (HP) technique. Stoichiometric mixtures of Na_2WO_4, WO_2 (99%, Rare Metallic), and WO_3 (99.999%, Rare Metallic) were ground in a mortar for 30–60 min and pressed into a pellet. The pellets were sealed in a platinum capsule, inserted in a graphite tube heater, and enclosed in a pyrophyllite cube. These procedures were carried out in a N_2-filled groove box. The Na_2WO_4 precursor was prepared by heating $Na_2WO_4{\cdot}2H_2O$ (99.8%), Alfa Aesar) in air at 400 °C for 24 h; a complete loss of water was checked by infrared spectroscopy.[31] The HP reactions were performed at 1000 °C for 30 min under pressures of 5–8 GPa. The samples were characterized through powder X-ray diffraction (XRD) with Cu Kα radiation at room temperature (RT). Synchrotron powder X-ray diffraction (SXRD) measurements were performed at RT on the BL02B2 beamline at SPring-8. The wavelengths employed were $\lambda = 0.42044$ Å for $x = 0.5, 0.6, 0.75, 1.0$ and $\lambda = 0.41914$ Å for $x = 0.8$. A glass capillary with a 0.2 mm inner diameter was used. The SXRD patterns were analyzed by the Rietveld refinement method using the program JANA2006.[32,33] Reaction procedures were similar to those followed for the synthesis of $Li_{0.5}WO_3$, with stoichiometric mixtures of Li_2WO_4 (99%, Kojundo Chemical), WO_2 (99%, Rare Metallic), and WO_3 (99.999%, Rare Metallic). Neutron diffraction (ND) measurements ($\lambda = 1.5397$ Å) for $Li_{0.5}WO_3$ were carried out using the high-resolution powder diffractometer BT-1 at the NIST Center for Neutron Research. The sample was loaded into a vanadium cell. The collected neutron data were analyzed by the program JANA2006.

Specific heat, C_p, was measured with a commercial calorimeter (Quantum Design PPMS) in a temperature range from 200 to 2 K. Thermal conductivity, κ, was measured by a standard four-contact method at temperatures between 300 and 100 K. Electrical resistivity, ρ, was measured with a four-probe method using a commercial apparatus (Quantum Design PPMS) equipped with an adiabatic demagnetization refrigerator. We used rectangular-shaped samples cut out from the pellets. Gold wires were attached to the samples with silver paste. Magnetization was measured with a SQUID magneto-meter (Quantum Design, MPMS).

RESULTS AND DISCUSSION

Figure 1a shows powder XRD patterns for a series of Na_xWO_3 at RT, which are indexed with a tetragonal supercell of a perovskite structure ($2a_p \times 2a_p \times 2c_p$) for $x \leq 0.75$ and a cubic supercell ($2a_p \times 2a_p \times 2a_p$) for $x \geq 0.8$, as indicated previously.[28,29] No impurity phases were detected for all samples. In Figure 1b, we plotted the x dependence of the reduced cell parameters, a_p, along with those of previous reports, where the samples were prepared by solid-state reaction at ambient pressure.[26–28] The results for $x \leq 0.8$ agree with the previous results. Whereas the reported data show a deviation from the Vegard law above $x = 0.85$, our samples follow a linear evolution in the entire range up to $x = 1$. Extrapolating the proposed relation, $a_p = 0.0819x + 3.7846$,[28] to $x = 1$ gives $a_p = 3.8665$ Å, which is fairly consistent with the experimental value of 3.86596(1) Å. This fact strongly suggests that previous studies overestimated the Na content for $x > 0.85$.[26–28] Deviation from the nominal values in earlier works may be due to Na evaporation. The use of high pressure prevented such undesirable evaporation. Higher compressibility of alkali metal may can also help Na ions be incorporated in the perovskite lattice.

A Rietveld refinement for the x =1 data assuming the $Im\bar{3}$ structure confirmed the full stoichiometry of our specimen, with reasonable reliability factors of R_{wp}= 7.37% and R_p = 5.70% and goodness-of-fit of 2.22 (Figure 2a and Table 1). Rietveld analyses for other Na_xWO_3 samples gave results consistent with nominal Na compositions (Figure S1 and Table S1). It is remarkable that ADP of the Na2 site for $NaWO_3$ ($x = 1$) is $2.23(15) \times 10^{-2}$ $Å^2$. This value corresponding to the isotropic root-mean-square displacement (rmsd) of 0.15(1) Å implies unusually large thermal vibration of sodium ions at the Na2 (6*b*) site. No anomaly is observed for the Na1 (2*a*) site (ADP = 7×10^{-3} $Å^2$).

Together with our previous report,[30] we have two *isoelectric* (d^1) compounds, $NaWO_3$ ($Im\bar{3}$) with $a^+a^+a^+$ rotations and KWO_3 ($Pm\bar{3}m$) with $a^0a^0a^0$ rotations. This offers an ideal opportunity to clarify the effect of WO_6 octahedral rotation on physical properties. First, let us present the temperature variation of resistivity, ρ, and magnetic susceptibility, χ (=M/H), in Figure 3. Both compounds exhibit metallic temperature dependence and almost the same ρ values in a whole temperature range examined (Figure 3a), where no signature of phase transition is observed. This behavior is paralleled with T-independent χ (Figure 3b), and hence, both compounds can be attributed to a Pauli paramagnetic metal. The Curie-type increases in χ at low temperatures below 20 K come from a small amount of free impurity spins (0.01–0.1%).

On the contrary, heat capacities of the two compounds behave differently, as shown in Figure 4a (C_p/T versus T). This difference can be highlighted for the C_p/T^3–T plot (Figure 4b). A broad peak is observed at 30 K only for $NaWO_3$, suggesting the presence of a low-energy optical phonon. A similar peak in the C_p/T^3 versus T curve has been known to appear in cage compounds having large ADPs:[9,34,35] these two features, namely, C_p/T^3 peak and large ADPs, are hallmarks of local vibrational mode (or rattling) associated with guest cations inside cages.[3,4] Thus, the observed broad peak of $NaWO_3$ is most likely attributed to Na2 (6*b*) ions with the large ADP.

The C_P/T^3 peak of cage compounds is typically characterized by Einstein specific heat within the "harmonic" approximation.[9,34,35] To do this, we analyzed our raw data of $NaWO_3$ by a combination of Debye and Einstein specific heats, along with an electronic specific heat of $C_e(T) = \gamma T$ (where γ is the electronic specific heat constant), which is given by

$$C_P(T) = \sum_i f_{D,i} C_{D,i}(T) + \sum_j f_{E,j} C_{E,j}(T) + C_e(T) \quad (1)$$

where $f_{D,i}$ and $f_{E,j}$ represent the number of the Debye and Einstein modes for the ith and jth contributions, respectively, all of which were determined by fitting. The sum of these is nothing but the total number of phonon modes in the unit cell, that is, $\sum_i f_{D,i} \sum_j f_{E,j} = 15$. $C_{D,i}(T)$ and $C_{E,j}(T)$ denote, respectively, Debye and Einstein specific heat, which are expressed as follows:

$$C_{D,i}(T) = 3R\left(\frac{T}{\Theta_{D,i}}\right)^3 \int_0^{\Theta_{D,i}/T} \frac{e^x x^4 dx}{(e^x - 1)^2} \quad (2)$$

$$C_{E,j}(T) = R\frac{e^{\Theta_{E,j}/T}}{\left(e^{\Theta_{E,j}/T} - 1\right)^2}\left(\frac{\Theta_{E,j}}{T}\right)^2 \quad (3)$$

Here, R is the gas constant and $\Theta_{D,i}$ and $\Theta_{E,j}$ are Debye and Einstein temperatures, respectively, that were also used as fitting parameters. The least-squares fitting was carried out using the data in the temperature range of 2 K < T < 200 K. A reasonable agreement was obtained for $NaWO_3$ when we assume two Debye and one Einstein modes ($i = 2$, $j = 1$) and for KWO_3 with two Debye modes only ($i = 2$, $j = 0$) (see Figure 4b and Table 2). It is clear that the additional Einstein term can reproduce the main feature of the C_P/T^3 peak in $NaWO_3$, suggesting rattling-like local vibrational mode. It is noteworthy that the introduction of Na site deficiency (i.e., $Na_{0.8}WO_3$) substantially suppresses the C_P/T^3 peak, as shown in Figure 4c. This implies that the effect of lattice defect and disorder is not the origin of the peak, as opposed to random or disordered systems such as those containing Bi or Pb with 6s lone pair electrons.[36,37]

The observed rattling phenomenon in $NaWO_3$ is unprecedented because the simple ABO_3 perovskite can be described by cubic closed-packed arrangement of AO_3 layers with B cations occupied at the interstitial octahedral site, and if the A cation is smaller, BO_6 octahedral rotation takes place to adjust and optimize the local coordination environment around A. In $NaWO_3$, however, the $a^+a^+a^+$ rotation generates nonequivalent Na sites, Na1 (2*a*) and Na2 (6*b*) (Figure 2b,c). This necessarily leads to a situation that both sites cannot be simultaneously optimized in terms of the local environment, yielding relatively large guest-free-space Δ around the Na2 ion. The value of Δ can be roughly estimated by taking the difference between the cage distance d_{cage} (from the center) and ionic radius of a guest cation: $\Delta = d_{cage} - r(Na^+)$. Our structural analysis indicates that Na1 has 12 equidistant Na1–O bonds (2.701(18) Å), whereas Na2 has four short (2.552(17) Å), four medium (2.778(17)

Å), and four long (2.916(17) Å) bonds (Figure 2d). The available space of Na1 and Na2 is estimated by calculating $d_{cage} = d - r(O^{2-})$,[9,24,34,35,38] where d is the Na–O bond length and $r(O^{2-})$ refers to the ionic radius of O^{2-} (=1.4 Å).[39] This yielded d_{cage} = 1.301 Å for Na1 and 1.152, 1.378, and 1.516 Å for Na2. Subsequently, using $r(Na^+)$ ~ 1 Å,[33] we obtained Δ ~ 0.3 Å for $Na1O_{12}$ and Δ ~ 0.5 Å for $Na2O_{12}$. The Δ value of $Na2O_{12}$ is parallel with those in the known cage compounds: Δ = 0.5–0.9 Å for filled skutterudites,[35,38] Δ = 0.3–0.4 Δ for A-site-ordered quadruple perovskites,[23,24] and Δ = 1–3 Å for clathrates and β-pyrochlores.[3,4,9,34] Together with the large rmsd of 0.15 Å, the large value of Δ for Na2 led us to conclude that the Na2 site is responsible for rattling local vibration.

A comparison with the A-site-ordered quadruple perovskite $CuCu_3V_4O_{12}$ further revealed that the coefficient of the Einstein specific heat, $f_{E,1}$ = 1.64 per the $NaWO_3$ formula, is larger than 0.27 per the "$CuVO_3$" formula (i.e., 1/4 × $CuCu_3V_4O_{12}$).[24,33] This result is fairly consistent with the difference in the rattling site: $CuCu_3V_4O_{12}$ has a rattler at the A site (2*a*) with the 2-fold multiplicity, whereas $NaWO_3$ has a rattler at the A′ site (6*b*) with 6-fold multiplicity. Another prominent feature that differentiates $NaWO_3$ from $CuCu_3V_4O_{12}$ is the degree of octahedral tilting. Although both compounds are isostructural, the octahedral ($a^+a^+a^+$) tilting in $CuCu_3V_4O_{12}$ is very extensive and gives the ∠V–O–V bridging angle of ~140°, which forces the A′ site transition metal to adopt the square-planar coordination. As a result, the A site can be a rattler. In contrast, the ∠W–O–W angle for $NaWO_3$ is ~169°, meaning that moderate octahedral rotation makes the A′ site a rattler.

One can generalize a strategy to find rattling phenomena in the pristine ABO_3 perovskite. Among 15 tilting systems in perovskite,[26,40–42] four systems ($a^+a^+a^+$, $a^0b^+b^+$, $a^0b^+c^-$, and $a^+a^+c^-$) have nonequivalent A sites. Examples include Li_xWO_3 ($x \le 0.5$) and $Li_{0.2}ReO_3$ with $a^+a^+a^+$,[43] $NaTaO_3$, $NaNbO_3$, $SrZrO_3$, and $SrHfO_3$ with $a^0b^+c^-$,[41,44] and NH_4MnCl_3 with $a^0b^+c^-$.[41] Unfortunately, most of them exist as an intermediate phase (e.g., 803–893 K for $NaTaO_3$). As far as we are aware, $Li_{0.5}WO_3$ with $a^+a^+a^+$ is stable at RT,[33] so we prepared the phase-pure $Li_{0.5}WO_3$ under high pressure and measured C_P. As expected, a C_P/T^3 peak is found at 20 IK, which can be fitted by introducing the Einstein specific heat with Θ_E = 98 K (Figure 4c and Figure S4 and Table S4). Extensive research on rattling compounds has shown that Θ_E decreases with increasing the cage size.[3,4,34,35,38] In fact, the smaller Θ_E value for $Li_{0.5}WO_3$ (versus 151 K for $NaWO_3$) could be related to a larger Δ value of ~1 Å.

In order to see the effect of rattling on physical properties, we measured κ for $NaWO_3$, the result of which is plotted in Figure 5, together with the data for KWO_3. The κ for $NaWO_3$ is clearly larger than that for KWO_3 in the whole temperature range measured. The Wiedemann–Franz law was used to extract the electronic contribution of thermal conductivity κ_e. Using the 200 K data of ρ, we obtained κ_e = 1.6 W/m·IK for $NaWO_3$ and κ_e = 2.2 W/m·K for KWO_3. Hence, the difference in κ is ascribed to that of lattice thermal conductivity, κ_L, but is different from what can be expected from the weight difference of K^+ and Na^+ ions.[45,46] We thus conclude that rattling vibration of Na^+ ions largely suppresses κ_L for $NaWO_3$. The suppression of κ_L is discussed for cage compounds in the context of the rattling effect.[13–15,46] More recently, the rattling and its relation with the suppression of κ_L

are discussed in compounds without cage structure[47,48] such as $LaOBiS_{2-x}Se_x$, where rattling-like local vibration is found in a cation at the planar coordination geometry with lone pair electrons. These findings give us hope to explore compounds beyond well-known cage systems toward finding low κ_L.

CONCLUSION

We have extended the solubility limit of Na_xWO_3 to the full stoichiometry ($x = 1$) by exploiting a high-pressure route. $NaWO_3$ crystallizes in a perovskite structure with all in-phase octahedral rotations ($a^+a^+a^+$). Despite the pristine perovskite phase, the specific heat measurement on $NaWO_3$ exhibits anharmonic phonon modes associated with low-energy rattling vibrations, which is absent in the ideal cubic perovskite KWO_3. The rattling behavior in $NaWO_3$ is caused by the presence of distinct crystallographic Na sites. The structural analysis revealed that the Na2 (6*b*) site is a rattler, as opposed to the isostructural quadruple $AA'_3B_4O_{12}$ perovskite, where the rattling site is the A (2*a*) cation. The present finding suggests that rattling phenomenon will be available for other ABO_3 perovskites with nonequivalent A sites. Conversely, a cation order may be possible by introducing different alkali metals (e.g, A = Na, A′ = K) in this structural type. Together with our recent study on stoichiometric phases of $K_{0.6}WO_3$ and KWO_3,[29] the high-pressure method turned out to be highly efficient: Li_xWO_3 ($0.5 \leq x \leq 1$) in the $LiNbO_3$ structure is also isolated.

Supplementary Material

Refer to Web version on PubMed Central for supplementary material.

ACKNOWLEDGMENTS

Synchrotron and neutron experiments were performed at SPring-8 BL02B2 of JASRI and BT-1 of the NIST Center for Neutron Research. We thank Dr. K Fujita for giving us heat capacity data of $CuCu_3V_4O_{12}$. The work was supported by CREST (JPMJCR1421) and JSPS KAKENHI (JP16H6439, 17H04849).

REFERENCES

(1). Nolas GS; Morelli DT; Tritt TM SKUTTERUDITES: A Phonon-Glass-Electron Crystal Approach to Advanced Thermoelectric Energy Conversion Applications. Annu. Rev. Mater. Sci 1999, 29, 89–115.

(2). Sato H; Sugawara H; Aoki Y; Harima H. Handook of Magnetic Materials; Elsevier: Amsterdam, 2009; Vol. 18, Chapter 1, p 1.

(3). Takabatake T; Suekuni K; Nakayama T; Kaneshita E. Phonon-glass Electron-crystal Thermoelectric Clathrates: Experiments and Theory. Rev. Mod. Phys 2014, 86, 669–716.

(4). Hiroi Z; Yamaura J; Hattori K. Rattling Good Super-conductor: β-Pyrochlore Oxides AOs_2O_6. J. Phys. Soc. Jpn 2012, 81, 011012.

(5). Nolas GS; Cohn JL; Slack GA; Schujman SB Semiconducting Ge Clathrates: Promising Candidates for Thermoelectric Applications. Appl. Phys. Lett 1998, 73, 178–180.

(6). Nolas GS; Poon J; Kanatzidis M. Recent Developments in Bulk Thermoelectric Materials. MRS Bull. 2006, 31, 199–205.

(7). Yonezawa S; Muraoka Y; Matsushita Y; Hiroi Z. Superconductivity in a Pyrochlore-related Oxide KOs_2O_6J. Phys. J. Phys.: Condens. Matter 2004, 16, L9–L12.

(8). Brühwiler M; Kazakov SM; Karpinski J; Batlogg B. Mass Enhancement, Correlations, and Strong-Coupling Superconductivity in the β-Pyrochlore KOs_2O_6. Phys. Rev. B: Condens. Matter Mater. Phys 2006, 73, 094518.

(9). Hiroi Z; Yonezawa S; Nagao Y; Yamaura J. Extremely Strong-coupling Superconductivity and Anomalous Lattice Properties in the β-Pyrochlore Oxide KOs_2O_6. Phys. Rev. B: Condens. Matter Mater. Phys 2007, 76, 014523.

(10). Sanada S; Aoki Y; Aoki H; Tsuchiya A; Kikuchi D; Sugawara H; Sato H. Exotic Heavy-Fermion State in Filled Skutterudite $SmOs_4Sb_{12}$. J. Phys. Soc. Jpn 2005, 74, 246–249.

(11). Hattori K; Hirayama Y; Miyake K. ILocal Heavy Quasiparticle in Four-Level Kondo Model. J. Phys. Soc. Jpn 2005, 74, 3306–3313.

(12). Hotta T. Effect of Rattling Phonons on Sommerfeld Constant. J. Phys. Soc. Jpn 2008, 77, 103711.

(13). Hotta T. Inverse Isotope Effect on Kondo Temperature in Electron-Rattling System. J. Phys. Soc. Jpn 2009, 78, 073707.

(14). Nolas GS; Slack GA; Morelli DT; Tritt TM; Ehrlich AC The effect of Rare-earth Filling on the Lattice Thermal Conductivity of Skutterudites. J. Appl. Phys 1996, 79, 4002–4008.

(15). Sales BC; Mandrus D; Williams RK Filled Skutterudite Antimonides: A New Class of Thermoelectric Materials. Science 1996, 272, 1325–1328. [PubMed: 8662465]

(16). Keppens V; Mandrus D; Sales BC; Chakoumakos BC; Dai P; Coldea R; Maple MB; Gajewski DA; Freeman EJ; Bennington S. Localized Vibrational Modes in Metallic Solids. Nature 1998, 395, 876–878.

(17). Koza MM; Johnson MR; Viennois R; Mutka H; Girard L; Ravot D. Breakdown of Phonon Glass Paradigm in La- and Ce-filled Fe_4Sb_{12} Skutterudites. Nat. Mater 2008, 7, 805–810. [PubMed: 18758457]

(18). Sleight AW; Gillson JL; Bierstedt PE High-temperature superconductivity in the $BaPb_{1-x}Bi_xO_3$ systems. Solid State Commun. 1975, 17, 27–28.

(19). Kuwahara H; Tomioka Y; Asamitsu A; Moritomo Y; Tokura Y. A First-Order Phase Transition Induced by a Magnetic Field. Science 1995, 270, 961–963.

(20). Megaw HD Origin of ferroelectricity in barium titanate and other perovskite-type crystals. Acta Crystallogr. 1952, 5, 739–749.

(21). Tilley RJD Perovskites: Structure–Property Relationships; John Wiley & Sons, Ltd.: Chichester, UK, 2016.

(22). Kageyama H; Hayashi K; Maeda K; Attfield JP; Hiroi Z; Rondinelli JM; Poeppelmeier KR Expanding frontiers in materials chemistry and physics with multiple anions. Nat. Commun 2018, 9, 772. [PubMed: 29472526]

(23). Akizuki Y; Yamada I; Fujita K; Nishiyama N; Irifune T; Yajima T; Kageyama H; Tanaka K. A-Site-Ordered Perovskite MnCu3V4O12 with a 12-Coordinated Manganese(II). Inorg. Chem 2013, 52, 11538–11543. [PubMed: 24028492]

(24). Akizuki Y; Yamada I; Fujita K; Taga K; Kawakami T; Mizumaki M; Tanaka K. Rattling in the Quadruple Perovskite $CuCu_3V_4O_{12}$. Angew. Chem., Int. Ed 2015, 54, 10870–10874.

(25). Shimakawa Y. A-Site-Ordered Perovskites with Intriguing Physical Properties. Inorg. Chem 2008, 47, 8562–8570. [PubMed: 18821822]

(26). Straumanis ME The Sodium Tungsten Bronzes. I., Chemical Properties and Structure. J. Am. Chem. Soc 1949, 71, 679–683.

(27). Brimm EO; Brantley JC; Lorenz JH; Jellinek MH Sodium and Potassium Tungsten Bronzes. J. Am. Chem. Soc 1951, 73, 5427–5432.

(28). Brown BW; Banks E. The Sodium Tungsten Bronzes. J. Am. Chem. Soc 1954, 76, 963–966.

(29). Clarke R New Sequence of Structural Phase Transitions in Na_xWO_3. Phys. Rev. Lett 1977, 39, 1550–1553.

(30). Ikeuchi Y; Takatsu H; Tassel C; Goto Y; Murakami T; Kageyama H. High-Pressure Synthesis of Fully Occupied Tetragonal and Cubic Tungsten Bronze Oxides. Angew. Chem., Int. Ed 2017, 56, 5770–5773.

(31). Fortes AD Crystal Structures of Spinel-Type Na_2MoO_4 and Na_2WO_4 Revisited using Neutron Powder Diffraction. Acta Cryst. E 2015, 71, 592–596.

(32). Petříček V; Dušek M; Palatinus L. Crystallographic Computing System JANA2006: General Features. Z. Kristallogr. - Cryst. Mater 2014, 229, 345–352.

(33). [See the Supporting Information for powder XRD and SXRD data of Na_xWO_3, the detailed structure analysis, and the analysis of the specific heat of Na_xWO_3, Li_xWO_3, and KWO_3.]

(34). Suekuni K; Avila MA; Umeo K; Fukuoka H; Yamanaka S; Nakagawa T; Takabatake T. Simultaneous Structure and Carrier Tuning of Dimorphic Clathrate $Ba_8Ga_{16}Sn_{30}$. Phys. Rev. B: Condens. Matter Mater. Phys 2008, 77, 235119.

(35). Matsuhira K; Sekine C; Wakeshima M; Hinatsu Y; Namiki T; Takeda K; Shirotani I; Sugawara H; Kikuchi D; Sato H. Systematic Study of Lattice Specific Heat of Filled Skutterudites. J. Phys. Soc. Jpn 2009, 78, 124601.

(36). Melot BC; Tackett R; O'Brien J; Hector AL; Lawes G; Seshadri R; Ramirez AP Large Low-temperature Specific Heat in Pyrochlore $Bi_2Ti_2O_7$. Phys. Rev. B: Condens. Matter Mater. Phys 2009, 79, 224111.

(37). Takatsu H; Hernandez O; Yoshimune W; Prestipino C; Yamamoto T; Tassel C; Kobayashi Y; Batuk D; Shibata Y; Abakumov AM; Brown CM; Kageyama H. Cubic Lead Perovskite $PbMoO_3$ with Anomalous Metallic Behavior. Phys. Rev. B: Condens. Matter Mater. Phys 2017, 95, 155105.

(38). Yamaura J; Hiroi Z. Rattling Vibrations Observed by Means of Single-Crystal X-ray Diffraction in the Filled Skutterudite ROs_4Sb_{12} (R = La, Ce, Pr, Nd, Sm). J. Phys. Soc. Jpn 2011, 80, 054601.

(39). Shannon RD Revised Effective Ionic Radii and Systematic Studies of Interatomic Distances in Halides and Chalcogenides. Acta Crystallogr., Sect. A: Cryst. Phys. Diffr., Theor. Gen. Crystallogr 1976, 32, 751–767.

(40). Woodward PM Octahedral Tilting in Perovskites. I. Structure Stabilizing Forces. Acta Crystallogr., Sect. B: Struct. Sci 1997, 53, 32–43.

(41). Woodward PM Octahedral Tilting in Perovskites. II. Structure Stabilizing Forces. Acta Crystallogr., Sect. B: Struct. Sci 1997, 53, 44–66.

(42). Howard CJ; Stokes HT Group-Theoretical Analysis of Octahedral Tilting in Perovskites. Acta Crystallogr., Sect. B: Struct. Sci 1998, 54, 782.

(43). Cava RJ; Santoro A; Murphy DW; Zahurak SM; Roth RS The Structures of the Lithium Inserted Metal Oxides $Li_{0.2}R.eO_3$ and $Li_{0.36}WO_3$. J. Solid State Chem 1983, 50, 121–128.

(44). Kennedy BJ; Howard CJ; Chakoumakos BC High-Temperature Phase Transitions in $SrHfO_3$. Phys. Rev. B: Condens. Matter Mater. Phys 1999, 60, 2972–2975.

(45). Tritt TM Thermal Conductivity: Theory, Properties, and Applications; Springer Science & Business Media: New York, 2005.

(46). Rowe DM CRC Handbook of Thermoelectrics; CRC Press: Boca Raton, FL, 1995.

(47). Suekuni K; Lee CH; Tanaka HI; Nishibori E; Nakamura A; Kasai H; Mori H; Usui H; Ochi M; Hasegawa T; Nakamura M; Ohira-Kawamura S; Kikuchi T; Kaneko K; Nishiate H; Hashikuni K; Kosaka Y; Kuroki K; Takabatake T. Retreat from Stress: Rattling in a Planar Coordination. Adv. Mater 2018, 30, 1706230.

(48). Lee CH; Nishida A; Hasegawa T; Nishiate H; Kunioka H; Ohira-Kawamura S; Nakamura M; Nakajima K; Mizuguchi Y. Effect of Rattling Motion without Cage Structure on Lattice Thermal Conductivity in $LaOBiS_{2-x}Se_x$. Appl. Phys. Lett 2018, 112, 023903.

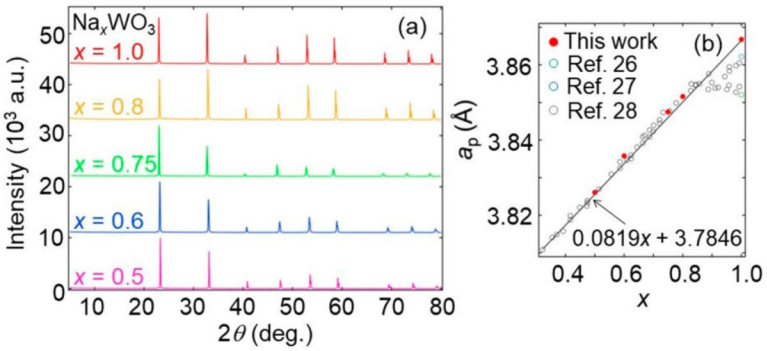

Figure 1.

(a) Powder XRD patterns of Na_xWO_3 measured at RT. (b) Pseudocubic (normalized) lattice parameters, a_p, plotted as a function of x, where data from previous studies[26–28] are included. The solid line represents the proposed relationship, $a_p(x) = 0.0819x + 3.7846$.[28]

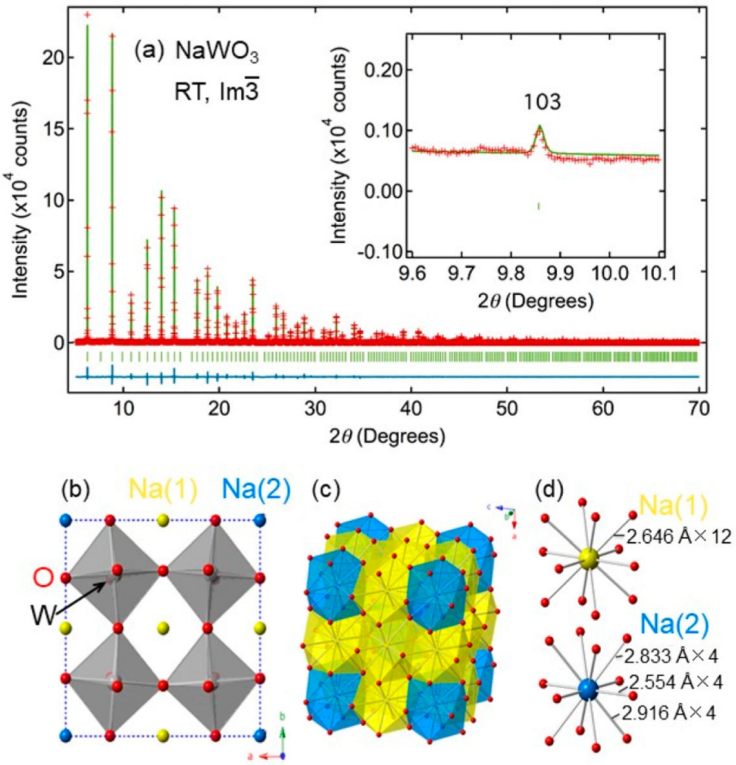

Figure 2.

(a) Rietveld refinement of SXRD of $NaWO_3$ at RT. Red crosses, green solid line, and blue solid line represent observed, calculated, and difference intensities, respectively. The green ticks are the position of Bragg peaks. The inset shows the (103) reflection. (b) Crystal structure of $NaWO_3$ ($Im\bar{3}$) with octahedral rotation of $a^+a^+a^+$. Blue, yellow, gray, and red spheres denote Na1 (2*a*), Na2 (6*b*), W (8*c*), and O (24*g*), respectively. The dotted lines show a $2a_p \times 2a_p \times 2a_p$ cell. (c) Two nonequivalent cuboctahedral units of NaO12 around Na1 (yellow) and Na2 (blue). (d) Coordination geometry around Na1 (top) and Na2 (bottom).

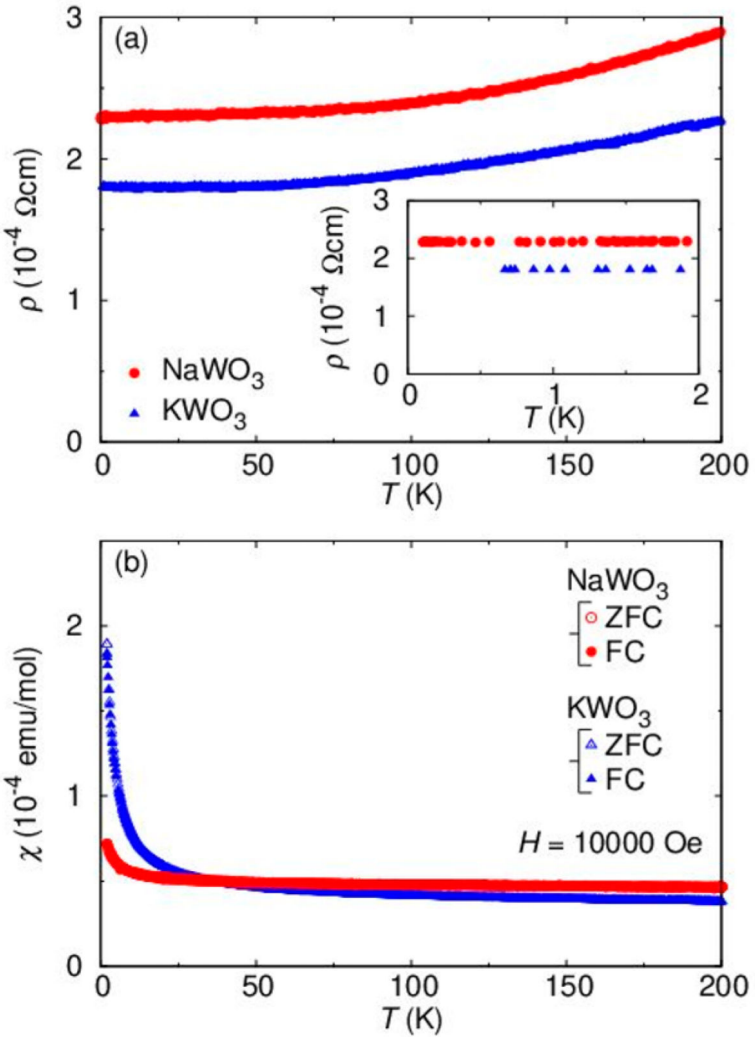

Figure 3.

(a) Temperature dependence of electrical resistivity, ρ, for 0.1 K < T < 200 K in $NaWO_3$ and 0.6 K < T < 200 K in KWO_3. The low-T region is magnified in the inset. (b) Temperature dependence of magnetic susceptibility, χ, for $NaWO_3$ and KWO_3 in the zero-field-and field-cooling process.

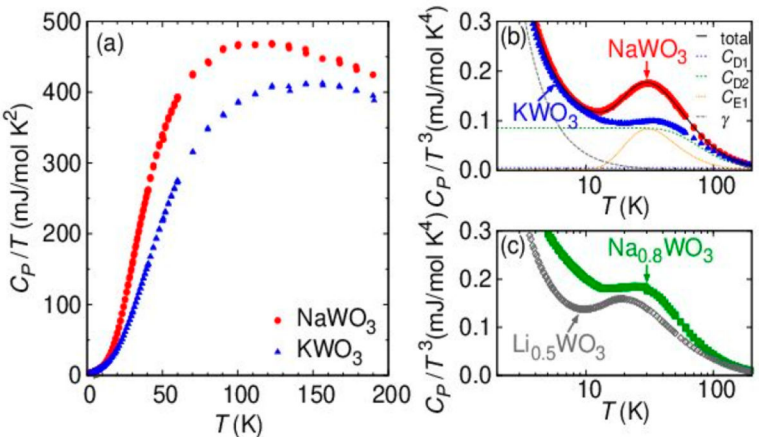

Figure 4.

(a) Temperature dependence of (a) C_P/T and (b) C_P/T^3 for $NaWO_3$ and KWO_3. Lines are fitting results (see the text for detail). (c) C_P/T^3 versus T plot for $Na_{0.8}WO_3$ and $Li_{0.5}WO_3$.

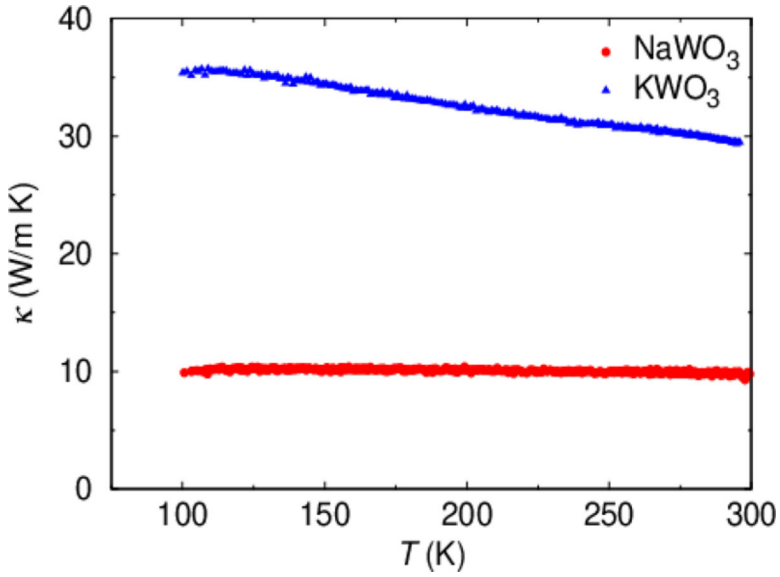

Figure 5.
Temperature dependence of thermal conductivity κ of $NaWO_3$ and KWO_3.

Table 1.

Refined Structural Parameters of Na_xWO_3 (x = 1.0) at RT (Space Group: $Im\bar{3}$ (No. 204), a = 7.731934(8) Å)

atom	site	*x*	*y*	*z*	U_{iso} (×10^{-2} Å^2)
Na	2*a*	0	0	0	0.7(2)
Na	6*b*	0	1/2	1/2	2.23(15)
W	8*c*	1/4	1/4	1/4	0.238(2)
O	24*g*	0	0.263(2)	0.230(2)	0.77(7)

Table 2.

Parameters Obtained by Fitting the Specific Heat Data of $NaWO_3$ to Equation 1, Where a Model with Two Debye and One Einstein Mode Was Used[a]

mode	$\Theta_{D,i}$	$\Theta_{E,j}$ (K)	$f_{D,i}$, $f_{E,j}$
D_1		962	6.62
D_2		371	6.74
E_1		151	1.64

[a]The terms of the Debye and Einstein modes are D_i (i = 1, 2) and E_1. The γ value was obtained as γ = 3.34 mJ/K^2.